IOPscience iopscience.iop.org

Home Search Collections Journals About Contact us My IOPscience

Effects of strong correlations on the disorder-induced zero-bias anomaly in the extended Anderson–Hubbard model

This article has been downloaded from IOPscience. Please scroll down to see the full text article.

2009 J. Phys.: Condens. Matter 21 385601

(http://iopscience.iop.org/0953-8984/21/38/385601)

View the table of contents for this issue, or go to the journal homepage for more

Download details:
IP Address: 129.252.86.83
The article was downloaded on 30/05/2010 at 05:26

Please note that terms and conditions apply.

J. Phys.: Condens. Matter **21** (2009) 385601 (13pp) doi:10.1088/0953-8984/21/38/385601

# Effects of strong correlations on the disorder-induced zero-bias anomaly in the extended Anderson–Hubbard model

**Yun Song[1], S Bulut[2], R Wortis[2] and W A Atkinson[2,3]**

[1] Department of Physics, Beijing Normal University, Beijing 100875, People's Republic of China
[2] Department of Physics and Astronomy, Trent University, 1600 West Bank Drive, Peterborough, ON, K9J 7B8, Canada
[3] Center for Electronic Correlations and Magnetism, EP VI, Universität Augsburg, D-86135 Augsburg, Germany

E-mail: billatkinson@trentu.ca

Received 2 June 2009, in final form 31 July 2009
Published 27 August 2009
Online at stacks.iop.org/JPhysCM/21/385601

**Abstract**

We study the effect of strong correlations on the zero-bias anomaly (ZBA) in disordered interacting systems. We focus on the two-dimensional extended Anderson–Hubbard model (EAHM) on a square lattice. The EAHM has both on-site and nearest-neighbour interactions and randomly chosen site energies. We use a mean-field theory that incorporates strong correlations and treats the disorder potential exactly. We use a simplified atomic-limit approximation for the diagonal inelastic self-energy that becomes exact in the large-disorder limit, and the off-diagonal self-energy is treated within the Hartree–Fock approximation. The validity of these approximations is discussed in detail. We find that strong correlations have a significant effect on the ZBA at half-filling, and enhance the ZBA gap when the interaction is finite ranged.

(Some figures in this article are in colour only in the electronic version)

## 1. Introduction

The term 'zero-bias anomaly' (ZBA) refers either to a peak in, or a suppression of, the density of states (DOS) at the Fermi energy. In disordered materials, a ZBA arises from the interplay between disorder and interactions. Zero-bias anomalies were originally predicted to occur in strongly disordered insulators by Efros and Shklovskii [1, 2] (ES) and later in weakly disordered metals by Altshuler and Aronov [3] (AA). In the limit of weak interactions and disorder, AA showed that the exchange self-energy of the screened Coulomb interaction produces a cusp-like minimum in the DOS at the Fermi energy. In the limit of strong disorder, ES showed that the classical Hartree self-energy of the unscreened Coulomb interaction causes the DOS to vanish at the Fermi energy. Experiments have shown a smooth evolution between the AA and ES limits as a function of disorder [4], and it appears that the essential physics of the ZBA in conventional metals and insulators is well understood.

In this work, we are interested in anomalies which have been observed in a number of transition metal oxide materials, where the physics is less well understood. Transition metal oxides often exhibit unconventional behaviour because the physics of their valence band is dominated by strong short-ranged interactions whose effects cannot generally be explained by conventional theories of metals and insulators. Most notably, many transition metal oxides exhibit a Mott transition when their valence band is half-filled. In disorder-free systems, the Mott transition [5, 6] occurs between a gapless metallic state and a gapped insulating state, and is driven by a strong intraorbital Coulomb interaction.

The Mott transition may occur as a function of any number of parameters [6], such as temperature [7] or magnetic field [8], but more commonly occurs in transition metal oxides as a result of chemical doping. A number of experiments [9–13] have found that chemical doping introduces sufficient disorder that there is a regime between the Mott-insulating and gapless phases that is characterized by a ZBA. This naturally raises the

 © 2009 IOP Publishing Ltd Printed in the UK

question of how the strong electron–electron correlations that are prevalent in the gapless phase near the Mott transition affect the physics of the ZBA.

The effect of strong correlations on the ZBA has received little attention[4]. In large part, this is due to the difficulty of incorporating both strong correlations and disorder in a manageable theory. A number of calculations based on the unrestricted Hartree–Fock approximation (HFA) have been used to study the phase diagram of the disordered Hubbard model [14–18], also known as the Anderson–Hubbard model (AHM). In these calculations, the disorder potential is treated exactly for finite-sized systems, but the intraorbital Coulomb interaction is treated at the mean-field level and therefore neglects strong correlations. Much of the recent progress has involved various formulations of dynamical mean-field theory (DMFT) to include disorder at some level of approximation. In particular, a number of authors have employed DMFT coupled with various effective medium approximations for the disorder potential [19–24]. In these calculations, the local electron self-energy contains both inelastic contributions from the interactions and elastic contributions from the disorder-averaging process. It is well known that these kinds of disorder-averaging approximations capture many features of the DOS but do not retain the nonlocal correlations responsible for the ZBA [3] and cannot, therefore, explain the experiments cited above. An extension of DMFT, called statistical DMFT, has been employed to study ensembles consisting of Bethe lattices with random site energies [25, 26]. This represents an improvement over the disorder-averaged approximations in that the results depend nontrivially on the coordination number of the Bethe lattice. Very recently, the DMFT equations have been solved by us on a two-dimensional square lattice in a way which preserves spatial correlations between sites [27]. The calculations employed a simple atomic-limit approximation for the self-energy that, while generally appropriate for the large-disorder limit, does not contain the off-diagonal self-energies responsible for the DOS anomalies observed in experiments.

In this work, we develop an extension of this method which includes the effect of the leading-order correction to the atomic-limit self-energy and we apply this method to both the AHM and extended Anderson–Hubbard model (EAHM). Agreement between our results for the AHM and the results of exact studies [28, 18] supports the method. Our primary result is in the context of the EAHM, where we find that strong correlations strongly enhance the ZBA. We argue that this is because the reduction in screening caused by strong correlations drives the system toward the strongly localized limit and ES-like behaviour.

Details of the calculations are given in section 2.1, while section 2.2 develops two key aspects of the reasoning behind our approach. First, because it is known to be deficient in the disorder-free limit, we demonstrate the validity of the Hubbard-I (HI) approximation for the intraorbital self-energy in the strongly disordered limit. Second, we show that the leading-order correction to the atomic-limit self-energy is nonlocal and has the form of an exchange self-energy. While this correction cannot be evaluated self-consistently at this level of approximation, the form of the correction suggests that the low-energy physics of the AHM may be reproduced via a particular mean-field treatment of the EAHM discussed in section 2.2. In section 2.3, we introduce a coherent potential approximation (CPA) for the disordered Hubbard model which is used as a point of comparison for our calculations. Numerical and analytical results for the case of a purely local self-energy (sections 3.1 and 3.3) provide context for our primary results, which include the nonlocal self-energy, presented in section 3.2.

[4] References [28] and [18] are notable exceptions.

## 2. Calculations

### 2.1. Method

The extended Anderson–Hubbard model is

$$\hat{H} = -t \sum_{\langle i,j\rangle,\sigma} c^{\dagger}_{i\sigma} c_{j\sigma} + \frac{V}{2} \sum_{\langle i,j\rangle} \hat{n}_i \hat{n}_j + \sum_i (\epsilon_i \hat{n}_i + U \hat{n}_{i\uparrow} \hat{n}_{i\downarrow}), \tag{1}$$

where $\langle i, j\rangle$ denotes nearest-neighbour lattice sites $i$ and $j$, $\hat{n}_{i\sigma} = c^{\dagger}_{i\sigma} c_{i\sigma}$, $\hat{n}_i = \hat{n}_{i\uparrow} + \hat{n}_{i\downarrow}$, and parameters $t$, $U$ and $V$ are the kinetic energy, the on-site Coulomb interaction, and the nearest-neighbour interaction respectively. $\epsilon_i$ is the site energy, which is box-distributed according to $P(\epsilon_i) = W^{-1}\Theta(W/2 - |\epsilon_i|)$, where $W$ is the width of the disorder distribution and $\Theta(x)$ the step function.

We treat the nearest-neighbour interaction at the mean-field level:

$$\frac{V}{2}\hat{n}_i\hat{n}_j \approx V\left(\hat{n}_i n_j - \sum_{\sigma} c^{\dagger}_{i\sigma} c_{j\sigma} f_{ji} + f_{ij}^2 - \frac{n_i n_j}{2}\right) \tag{2}$$

with $f_{ji} = \langle c^{\dagger}_{j\uparrow} c_{i\uparrow}\rangle = \langle c^{\dagger}_{j\downarrow} c_{i\downarrow}\rangle$ in the paramagnetic phase and $n_j = \langle \hat{n}_j\rangle$. Both $f_{ij}$ and $n_j$ are determined self-consistently. The mean-field Hamiltonian, up to an additive constant, is:

$$\hat{H} = \sum_{\langle i,j\rangle\sigma} t'_{ij} c^{\dagger}_{i\sigma} c_{j\sigma} + \sum_i \epsilon'_i \hat{n}_i + U \sum_i \hat{n}_{i\uparrow}\hat{n}_{j\downarrow} \tag{3}$$

where $t'_{ij} = -t - V f_{ij}$ and $\epsilon'_i = \epsilon_i + V \sum_j n_j$, where the sum is over nearest neighbours of $i$.

The approximate Hamiltonian (3) is then solved using an iterative mean-field theory that captures the strong correlation physics of the intraorbital interaction and treats the disorder potential exactly for each realization of disorder. The theory can be formulated in analogy to existing formulations of DMFT specifically designed for inhomogeneous systems[5]; however, our choice of the HI approximation for the self-energy leads to different low-energy physics than found in conventional DMFT, and we therefore label our method 'Hubbard mean-field theory' (HMFT) to avoid confusion[6].

On an $N$-site lattice, the single-particle Green's function can be expressed as an $N \times N$ matrix in the site index:

$$\mathbf{G}(\omega) = [\omega\mathbf{I} - \mathbf{t} - \boldsymbol{\epsilon} - \boldsymbol{\Sigma}(\omega)]^{-1} \tag{4}$$

[5] Similar real-space formalisms have been employed by others to describe heterostructures, notably [29]. A similar formalism has also been applied to the disordered Bethe lattice in [25, 26] where it was termed 'statistical DMFT'.

[6] Note that the method is closely related to that in [27] where the name 'statistical DMFT' was used.

with $\mathbf{I}$ the identity matrix, $\mathbf{t}$ the matrix of renormalized hopping amplitudes $t'_{ij}$, $\boldsymbol{\epsilon}$ the diagonal matrix of renormalized site energies $\epsilon'_i$ and $\boldsymbol{\Sigma}(\omega)$ the matrix of local self-energies. The self-energy $\Sigma_i(\omega)$ corresponds to the inelastic self-energy $\Sigma(\omega)$ (the so-called 'impurity self-energy') in standard DMFT, which may be obtained by various self-consistent impurity solvers [30]. The iteration cycle begins with the calculation of $\mathbf{G}(\omega)$ from (4), and $n_{i\sigma}$ and $f_{ij}$ given by,

$$n_{i\sigma} = -\frac{1}{\pi}\int_{-\infty}^{\varepsilon_F} \mathrm{d}\omega\ \mathrm{Im}\, G_{ii}(\omega) \tag{5}$$

$$f_{ij} = -\frac{1}{\pi}\int_{-\infty}^{\varepsilon_F} \mathrm{d}\omega\ \mathrm{Im}\, G_{ji}(\omega) \tag{6}$$

from the previous iteration. For each site $i$, one defines a Weiss mean field $\mathcal{G}_i^0(\omega) = [G_{ii}(\omega)^{-1} + \Sigma_i(\omega)]^{-1}$ where $G_{ij}(\omega)$ are the matrix elements of $\mathbf{G}(\omega)$. The HI approximation is the simplest improvement over the HFA that generates both upper and lower Hubbard bands and, as we discuss in section 2.2, it works well in the large-disorder limit $W \gg t$. In this approximation, $\mathcal{G}_i(\omega) = [\mathcal{G}_i^0(\omega)^{-1} - \Sigma_i^{\mathrm{HI}}(\omega)]^{-1}$ where

$$\Sigma_i^{\mathrm{HI}}(\omega) = U\frac{n_i}{2} + \frac{U^2\frac{n_i}{2}(1-\frac{n_i}{2})}{\omega - \epsilon'_i - U(1-\frac{n_i}{2})}, \tag{7}$$

and $n_i$ is self-consistently determined for each site.

We remark that we can also express the Green's function as

$$\mathbf{G}(\omega) = [\omega\mathbf{I} - \mathbf{t_0} - \boldsymbol{\epsilon}_0 - \boldsymbol{\Sigma}(\omega)]^{-1} \tag{8}$$

where $\mathbf{t_0}$ and $\boldsymbol{\epsilon_0}$ are matrices of the unrenormalized hopping amplitudes and site energies. In this case, the self-energy is:

$$\Sigma_{ii} = U\frac{n_i}{2} + V\sum_j n_j + \frac{U^2\frac{n_i}{2}(1-\frac{n_i}{2})}{\omega - \epsilon_i - U(1-\frac{n_i}{2}) - V\sum_j n_j} \tag{9a}$$

and

$$\Sigma_{ij} = -Vf_{ij}. \tag{9b}$$

This form emphasizes the nonlocal nature of the self-energy. In (9*a*) and (9*b*), $-Vf_{ij}$ is the exchange self-energy, and $V\sum_j n_j$ is the Hartree contribution to the self-energy.

We finish this section with a remark on the different assumptions implicit in HMFT and conventional (single-site) DMFT. In DMFT, the self-energy is purely local and is based on a mapping of the Hubbard model onto an ensemble of Anderson-impurity Hamiltonians. DMFT therefore assumes that the most important low-energy inelastic scattering processes involve Kondo scattering of bath electrons. This assumption is exact in infinite dimensions, but there are indications that it fails in two dimensions: recent cluster DMFT calculations find that the Kondo resonance is absent in two dimensions when the cluster size is larger than 1 [31], and exact finite-size numerical studies in the limit of large disorder do not see evidence of Kondo physics [28, 32]. HMFT, by contrast, assumes that intersite coupling is small enough (in this case due to disorder) that Kondo physics is not relevant, but that the atomic limit is a useful starting point. This perspective is motivated by the following observation: the local noninteracting Green's function for any lattice can always be written [30]

$$G_{ii}(\omega) = \frac{1}{\omega - \epsilon_i - \Lambda_i(\omega)}$$

where $\Lambda_i(\omega)$ is the hybridization function that describes the coupling between the $i$th lattice site and the rest of the lattice. It follows directly from perturbation theory in the disordered limit that $\Lambda_i(\omega) \sim Z_c t^2/W \ll t$, where $Z_c$ is the coordination number. $G_{ii}(\omega)$ is therefore weakly perturbed from the atomic limit when $W$ is large and $Z_c$ is small. In section 2.2, we show that, when $Z_c t/W$ is small, the leading-order correction to the atomic-limit self-energy is nonlocal. The different assumptions of HMFT and DMFT thus lead to different physics: in HMFT, the nonlocal self-energy correction produces a reduction of the DOS at $\varepsilon_F$ while, in DMFT, the Kondo scattering generates a peak in the DOS at $\varepsilon_F$.

### 2.2. *Validity of the self-energy*

The goal of this section is to examine critically our treatment of the Hubbard-$U$ interaction in section 2.1. We begin by showing that the HI treatment of $U$ is valid in the limit of large disorder and low coordination number, resulting in a purely local self-energy. We then show that the leading-order correction to $\Sigma(\omega)$ arising from $U$ is nonlocal and has the form of an exchange self-energy. We argue that it is thus possible to develop a qualitative understanding of the ($V = 0$) Anderson–Hubbard model using a modified version of the self-energy where (i) the Hartree contributions are dropped from (9*a*) and (ii) $V \to V_{\mathrm{eff}} \sim 2t$ in (9*b*).

Our discussion is based on a two-site Anderson–Hubbard Hamiltonian, i.e. on (3) with two sites labelled '1' and '2'. This Hamiltonian can, of course, be diagonalized exactly with relatively little effort. Here, we are interested in developing an approximate treatment that is valid in the large-disorder limit, and which can be applied to the $N$-site problem. Comparison to the exact solution is used as a benchmark for the approximation.

We use an equation-of-motion method to arrive an approximate expression for the single-particle Green's function. Defining a Liouvillian superoperator $\mathcal{L}$ such that [33]

$$\mathcal{L}\hat{A} \equiv [\hat{H}, \hat{A}], \tag{10}$$

where $\hat{A}$ is an arbitrary operator, we can formally write the time evolution of $\hat{A}$ as $\hat{A}(t) = \exp(\mathrm{i}\mathcal{L}t)\hat{A}(0)$. It follows directly that the retarded Green's function can be written

$$G_{i\sigma,j\sigma}(\omega) = \left(c_{i\sigma}^\dagger \left| \frac{1}{\omega - \mathcal{L}} c_{j\sigma}^\dagger \right.\right) \tag{11}$$

where the inner product of two operators is defined as $(\hat{A}|\hat{B}) = \langle\{\hat{A}^\dagger, \hat{B}\}\rangle$ and $\{,\}$ refers to the anticommutator. The operator set $c_{i\sigma}^\dagger$ is not closed under operations by $\mathcal{L}$, but a complete operator set can be generated with repeated operation by $\mathcal{L}$ on $c_{i\sigma}^\dagger$. For example,

$$\mathcal{L}c_{i\sigma}^\dagger = \epsilon'_i c_{i\sigma}^\dagger + \sum_j c_{j\sigma}^\dagger t'_{ji} + U(b_{i\sigma}^\dagger - c_{i\sigma}^\dagger n_{i\bar{\sigma}}) \tag{12}$$

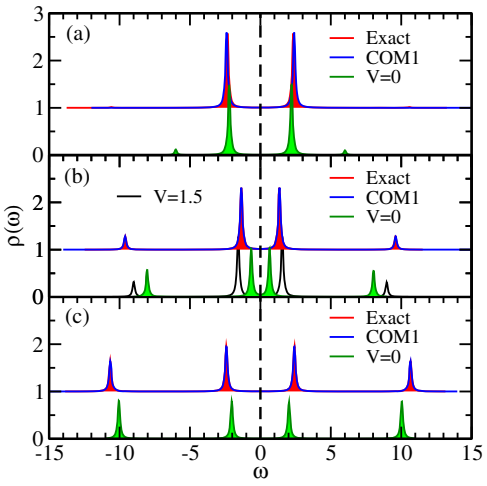


**Figure 1.** Comparison of the approximate and exact densities of states for a two-site system. The site energies are $\epsilon_1 = W/2$, $\epsilon_2 = -W/2$ for $W = 8t$. Figure panels are for (a) $U = 4t$, (b) $U = 8t$ and (c) $U = 12t$. Exact calculations are based on exact diagonalization of the two-site Hubbard model. Approximate densities of states are given by $\rho(\omega) = -\operatorname{Im}\sum_i G_{ii}(\omega)/\pi$, with $\mathbf{G}(\omega)$ the matrix (19). Two different approximations are made for the self-energies: the first has the self-energy given by (20*a*) and (20*b*) and makes the COM1 approximation for $p$ [36]; the second has the self-energy given by (9*a*) and (9*b*) with different choices for $V$. Both the COM1 and exact solutions are offset for clarity. The COM1 solution is essentially indistinguishable from the exact solution in all cases. Note that $\varepsilon_F$ is the zero of energy in this and all other figures.

where $b^\dagger_{i\sigma} = c^\dagger_{i\sigma}(\hat{n}_{i\bar{\sigma}} - n_{i\bar{\sigma}})$ and $\bar{\sigma} = -\sigma$. The operator $b^\dagger_{i\sigma}$ is a composite operator, and further composite operators can be generated from $\mathcal{L}^2 c^\dagger_{i\sigma}$, etc. The higher-order composite operators involve excitations on multiple lattice sites, and are therefore expected to be less important in the disordered case than in the clean limit. Here, we truncate the series after a single application of $\mathcal{L}$ so that our operator basis consists of two operators, $c^\dagger_{i\sigma}$ and $b^\dagger_{i\sigma}$, for each site and spin. This leads to a 'two-pole' approximation for the Green's function. This approach has been studied at length in the clean limit and has been shown to provide a reasonable qualitative description of the Hubbard model [34–36]. As shown in figure 1, the two-pole approximation (described in more detail below) is essentially indistinguishable from the exact solution for the DOS of the two-site system.

It is useful to define a generalized Green's function in the expanded operator space:

$$\mathcal{G}_{i\sigma,j\sigma}(\omega) = \begin{bmatrix} (c^\dagger_{i\sigma}|\frac{1}{\omega-\mathcal{L}}c^\dagger_{j\sigma}) & (c^\dagger_{i\sigma}|\frac{1}{\omega-\mathcal{L}}b^\dagger_{j\sigma}) \\ (b^\dagger_{i\sigma}|\frac{1}{\omega-\mathcal{L}}c^\dagger_{j\sigma}) & (b^\dagger_{i\sigma}|\frac{1}{\omega-\mathcal{L}}b^\dagger_{j\sigma}) \end{bmatrix} \tag{13}$$

such that $G_{i\sigma,j\sigma}(\omega)$ is given by the upper left quadrant of $\mathcal{G}_{i\sigma,j\sigma}(\omega)$. Defining the Liouvillian matrix,

$$L_{i\sigma,j\sigma}(\omega) = \begin{bmatrix} (c^\dagger_{i\sigma}|\mathcal{L}c^\dagger_{j\sigma}) & (c^\dagger_{i\sigma}|\mathcal{L}b^\dagger_{j\sigma}) \\ (b^\dagger_{i\sigma}|\mathcal{L}c^\dagger_{j\sigma}) & (b^\dagger_{i\sigma}|\mathcal{L}b^\dagger_{j\sigma}) \end{bmatrix}, \tag{14}$$

and the matrix of overlap integrals,

$$\chi_{i\sigma,j\sigma} = \begin{bmatrix} (c^\dagger_{i\sigma}|c^\dagger_{j\sigma}) & (c^\dagger_{i\sigma}|b^\dagger_{j\sigma}) \\ (b^\dagger_{i\sigma}|c^\dagger_{j\sigma}) & (b^\dagger_{i\sigma}|b^\dagger_{j\sigma}) \end{bmatrix}, \tag{15}$$

we get

$$\mathcal{G}_{i\sigma,j\sigma}(\omega) = \sqrt{\chi_{i\sigma,i\sigma}}[\omega - \tilde{L}]^{-1}_{i\sigma,j\sigma}\sqrt{\chi_{j\sigma,j\sigma}} \tag{16}$$

with

$$\chi_{i\sigma,j\sigma} = \delta_{i,j}\begin{bmatrix} 1 & 0 \\ 0 & n_{i\bar{\sigma}}(1-n_{i\bar{\sigma}}) \end{bmatrix} \tag{17}$$

and $\tilde{L} = \sqrt{\chi^{-1}}L\sqrt{\chi^{-1}}$.

For the nonmagnetic case, up and down spins are equivalent, and only the former need be considered. For the two-site system, and taking the basis $[c^\dagger_{1\uparrow}, c^\dagger_{2\uparrow}, b^\dagger_{1\uparrow}, b^\dagger_{2\uparrow}]$, we write the Liouvillian matrix explicitly as

$$\tilde{L} = \begin{bmatrix} \epsilon'_1 + Un_{1\downarrow} & -t' & \tilde{U}_1 & 0 \\ -t' & \epsilon'_2 + Un_{2\downarrow} & 0 & \tilde{U}_2 \\ \tilde{U}_1 & 0 & \tilde{\epsilon}_1 & -t'\tilde{p} \\ 0 & \tilde{U}_2 & -t'\tilde{p} & \tilde{\epsilon}_2 \end{bmatrix}, \tag{18}$$

where

$$\tilde{U}_i = U\sqrt{n_{i\downarrow}(1-n_{i\downarrow})} \qquad \tilde{\epsilon}_i = \epsilon'_i + U(1-n_{i\downarrow}) - t'\tilde{\Delta}_i$$

$$\tilde{\Delta}_i = \Delta_i[n_{i\downarrow}(1-n_{i\downarrow})]^{-1}$$

$$\Delta_i = \langle(\hat{n}_{i\uparrow} - n_{i\downarrow})c^\dagger_{j\downarrow}c_{i\downarrow}\rangle - \langle(1-\hat{n}_{i\uparrow} - n_{i\downarrow})c^\dagger_{i\downarrow}c_{j\downarrow}\rangle$$

$$\tilde{p} = p[n_{1\downarrow}(1-n_{1\downarrow})n_{2\downarrow}(1-n_{2\downarrow})]^{-1/2}$$

$$p = \langle\hat{n}_{1\downarrow}\hat{n}_{2\downarrow}\rangle - n_{1\downarrow}n_{2\downarrow} - \langle c^\dagger_{1\uparrow}c_{2\uparrow}(c^\dagger_{2\downarrow}c_{1\downarrow} + c^\dagger_{1\downarrow}c_{2\downarrow})\rangle.$$

In the expression for $\Delta_i$, $j$ is the nearest neighbour to $i$ (i.e. $j = 1$ if $i = 2$ and $j = 2$ if $i = 1$).

Equation (18) allows us to solve for the Green's function, provided the fields $\Delta_i$, $p$, and $n_{i\downarrow}$ are known. In practice, $\Delta_i$ and $n_{i\downarrow}$ can be solved self-consistently, but further information is needed to calculate $p$.

The Green's function $G(\omega)$ is given by the upper left $2\times 2$ quadrant of $\mathcal{G}(\omega)$. It is straightforward to solve (16) to show that

$$G(\omega) = \begin{bmatrix} \omega - \epsilon'_1 - \Sigma_{11}(\omega) & t' - \Sigma_{12}(\omega) \\ t' - \Sigma_{21}(\omega) & \omega - \epsilon'_2 - \Sigma_{22}(\omega) \end{bmatrix}^{-1} \tag{19}$$

with

$$\Sigma_{ii} = Un_{i\downarrow} + \frac{\tilde{U}_i^2(\omega - \tilde{\epsilon}_j)}{(\omega-\tilde{\epsilon}_1)(\omega-\tilde{\epsilon}_2) - t'^2\tilde{p}^2} \tag{20a}$$

$$\Sigma_{12} = \Sigma_{12} = \frac{-t'U^2p}{(\omega-\tilde{\epsilon}_1)(\omega-\tilde{\epsilon}_2) - t'^2\tilde{p}^2} \tag{20b}$$

where $j$ is again the nearest neighbour to $i$. Equations (20*a*) and (20*b*) are the basic expressions for the self-energy. These expressions are shown in figure 1 to give very accurate results for the Green's function provided that $p$ is correctly chosen. In this work, we have used the COM1 approximation of Avella and Mancini [36]. The COM1 approximation works well for the simple inhomogeneous systems we have tested it on, but is extremely difficult to apply to disordered systems where $p$ is different along every bond in the lattice.

Some simplifications can be made in the case of large disorder. To begin with, we discuss the diagonal self-energies $\Sigma_{ii}$, and take $i = 1$. We note that $\tilde{p} \sim O(1)$, so that

$$\Sigma_{11} \to U n_{1\downarrow} + \frac{U^2 n_{1\downarrow}(1 - n_{1\downarrow})}{\omega - \epsilon_1' - U(1 - n_{1\downarrow}) + t'\tilde{\Delta}_1}, \qquad (21)$$

whenever $(\omega - \tilde{\epsilon}_1)(\omega - \tilde{\epsilon}_2) \gg t^2$. Apart from the shift $t'\tilde{\Delta}_1$, this is just the Hubbard-I approximation for the self-energy. As we show next, (21) is justified for $\omega \approx \varepsilon_F$ in the large-disorder limit, which corresponds in the two-site problem to $|\epsilon_1 - \epsilon_2| \gg t$.

We are interested in the validity of (21) near $\varepsilon_F$ and take the particular case $\varepsilon_F = U/2$ (which corresponds to half-filling) where strong correlations are most important. When $t = 0$, each atomic Green's function has poles at $\epsilon_i'$ and $\epsilon_i' + U$, so that spectral weight at $\varepsilon_F$ comes from sites with $\epsilon_i' = \pm U/2$. This remains approximately true when $t \neq 0$ provided that $W \gg t$. Then, if site 1 contributes spectral weight at the Fermi level,

$$\varepsilon_F - \tilde{\epsilon}_1 \sim U,$$

and (21) follows from (20*a*) provided $|\varepsilon_F - \tilde{\epsilon}_2| > t^2/U$. This condition will only not be met when $\epsilon_2' \approx -U/2$. In other words, the two cases not well described by (21) are (i) $\epsilon_1' \approx \epsilon_2'$ and (ii) $\epsilon_1' \approx \epsilon_2' + U$.

Certainly, in any randomly distributed set of site energies, both cases are expected to occur for some fraction of sites on the lattice. However, if the disorder potential is large, and the coordination number of the lattice is low, then the probability of any given site having a nearest neighbour satisfying either condition (i) or (ii) is low, and the fraction of sites not described by (21) is small. It is interesting to note that the physical processes neglected here are (i) formation of singlet correlations between nearly degenerate sites and (ii) resonant exchange between sites in which the double occupancy of site 1 is nearly degenerate with singlet formation between sites 1 and 2.

Two further comments are warranted regarding our treatment of $\Sigma_{11}$. First, the simplifications made above assume that both $U$ and $W$ are large. This case is directly relevant to the current work since it is the regime in which density of states anomalies are observed. However, we have found empirically through numerical studies of small clusters that (21) is also a good approximation when $U$ is small. This point is illustrated in figure 1(a). Second, the term $t'\Delta_1$ in (21) is neglected in (9*a*). In the clean limit, $|\Delta| \lesssim 0.2$ and depends only weakly on $U$ [36]. This term is small relative to the Hartree shift $V\sum_j n_j$ and is therefore neglected.

We emphasize that the Hartree shift does not arise in our perturbative treatment of the Hubbard-$U$ interaction. It must therefore be understood to come directly from the nonlocal Coulomb interaction. This point is important because, as is shown in section 3, the Hartree term makes a large contribution to the ZBA at half-filling.

The off-diagonal self-energy, (20*b*), is significantly harder to evaluate than the diagonal term. It requires knowledge of a quantity $p$ that cannot be calculated self-consistently within the two-pole approximation, although various approximations exist [36]. However, we note from the definition of $p$ that $\Sigma_{12}$ measures exchange correlations between sites 1 and 2 and plays a similar role to the exchange self-energy $-Vf_{12}$ defined in section 2.1. The form of (20*b*) therefore suggests that the off-diagonal self-energy can be represented qualitatively by a mean-field exchange self-energy due to an effective nonlocal interaction $V_{\text{eff}}$. We make a rough estimate of $V_{\text{eff}}$ as follows: consider the case where site 1 contributes spectral weight slightly below $\varepsilon_F$. There are two possible ranges of site energies for which this occurs: $\epsilon_1$ less than but approximately equal to $\varepsilon_F$, and $\epsilon_1$ less than but approximately equal to $\varepsilon_F - U$. In the first case, $n_1 \approx 1$ and the exchange self-energy is largest for sites 2 which have $n_2 \approx 0$, or $\epsilon_2 \gtrsim \varepsilon_F$ [37]. At half-filling ($\varepsilon_F = U/2$), (20*b*) simplifies to $\Sigma_{12}(\varepsilon_F) \approx -2tp$ (where we have used the fact that $\tilde{p} \approx 0$) and

$$V_{\text{eff}} \sim 2t. \qquad (U, W \gg t). \qquad (22)$$

A similar expression is found when $\epsilon_1 \approx \varepsilon_F - U$. Equation (22) is remarkable because it depends on neither $U$ nor $W$.

Figure 1 shows the DOS of a two-site system calculated within the approximation given by (9*a*) and (9*b*). The main effect of $V$ is to produce a level repulsion between states above and below the Fermi energy, as illustrated in figure 1(b). The magnitude of the level repulsion decreases with increasing $U$, and is unobservably small for $U = 12t$ and $V < 3t$. As the figure shows, the DOS is well reproduced with $V = 0$ when $U \ll W$ and $U \gg W$, but is much less well reproduced when $U \approx W$. As expected from the analysis above, this can be corrected to some extent by a judicious choice of $V$.

Finally, we note that the nonlocal self-energy plays a crucial role in the clean low-dimensional Hubbard model [38–41]. It is often treated explicitly in the large-$U$ limit via an approximate mapping of the Hubbard model onto the $t$–$J$ model, where $J$ is the strength of the effective nonlocal interaction. A major difference between the $t$–$J$ model and the AHM is that double occupation of orbitals is completely suppressed in the former whereas a finite fraction of sites are doubly occupied in the latter when $W \gtrsim U$. A second difference is that the effective interaction in the $t$–$J$ model is a spin–spin interaction with $J \sim t^2/U$, whereas the self-energy correction derived here has the structure of an exchange self-energy and is proportional to $t$. The apparent distinction between the Hubbard model and AHM has been noted in [28], where exact numerical calculations found a ZBA that is nearly independent of $U$ and linearly proportional to $t$ (consistent with (22)).

### 2.3. Coherent potential approximation

In this section, we describe an implementation of the coherent potential approximation (CPA) that includes the effects of interactions and disorder within an effective medium approximation. As mentioned in the introduction, the CPA neglects spatial correlations and therefore misses the physics of the ZBA. It is therefore useful as a point of comparison for our HMFT calculations.

Our CPA implementation applies specifically to the HFA and the HI approximation, and hence is denoted by HFA + CPA or HI + CPA as appropriate, and reduces to these approximations in the limit $W \to 0$. The HFA + CPA and HI + CPA algorithms also reduce to the usual CPA in the noninteracting $U \to 0$ limit. Because of the local nature of these approximations, the nonlocal interaction $V$ has not been included.

For a particular lattice, we can calculate the local Green's function of the disorder-averaged system:

$$G_{\rm loc}(\omega) = \frac{1}{N}\sum_{\mathbf{k}} \frac{1}{\omega - \epsilon_k - \Sigma(\omega)}. \tag{23}$$

In this equation, $\Sigma(\omega)$ is a self-energy that includes both inelastic contributions from the local interaction and elastic contributions from the disorder scattering. On the first iteration of the algorithm, $\Sigma(\omega)$ is guessed, and on later iterations it is taken from the output of the previous iterations. Next, we define a Green's function

$$G_\epsilon(\omega) = [[G_{\rm loc}(\omega)]^{-1} + \Sigma(\omega) - \epsilon - \Sigma_\epsilon(\omega)]^{-1}. \tag{24}$$

This is the local Green's function for a site with energy $\epsilon$ which is embedded in the effective medium. The term $\Sigma_\epsilon(\omega)$ is the *inelastic* self-energy for the site, and must be determined self-consistently. For both the HFA and HI approximation, $\Sigma_\epsilon(\omega)$ depends on the local charge density $n_\epsilon$. Equation (24) can therefore be closed by the relations

$$n_\epsilon = -\frac{2}{\pi}\int_{-\infty}^{\varepsilon_{\rm F}} {\rm Im}\, G_\epsilon(\omega)\, {\rm d}\omega, \tag{25}$$

and $\Sigma_\epsilon(\omega) = U\frac{n_\epsilon}{2}$ for the HFA or

$$\Sigma_\epsilon(\omega) = U\frac{n_\epsilon}{2} + \frac{U^2\frac{n_\epsilon}{2}(1-\frac{n_\epsilon}{2})}{\omega - \epsilon - U(1-\frac{n_\epsilon}{2})} \tag{26}$$

for the HI approximation. Equations (24)–(26) must be iterated to convergence for each value of $\epsilon$.

We then average $G_\epsilon(\omega)$ over site energies to get

$$G_{\rm av}(\omega) = \frac{1}{W}\int_{-W/2}^{W/2} {\rm d}\epsilon\, G_\epsilon(\omega), \tag{27}$$

and a new self-energy is found via

$$\Sigma^{\rm new}(\omega) = [G_{\rm loc}(\omega)]^{-1} + \Sigma(\omega) - [G_{\rm av}(\omega)]^{-1}. \tag{28}$$

The iteration cycle is now restarted at (23) with $\Sigma^{\rm new}(\omega)$ taking the place of $\Sigma(\omega)$. The iteration process is terminated when the difference between $\Sigma^{\rm new}(\omega)$ and $\Sigma(\omega)$ is small. When the iteration cycle is complete, $G_{\rm loc}(\omega)$ is the disorder-averaged Green's function of the interacting system.

## 3. Results

In this section, we present our numerical density of states results and examine in particular how different pieces of the self-energy (9*a*) and (9*b*) influence the ZBA. In section 3.1, we show results for the case where the self-energy is purely local, achieved by setting $V = 0$ in (9*a*) and (9*b*). An analytical discussion of these results is presented in section 3.3. In section 3.2, we begin by exploring the effects of including an exchange contribution to the self-energy, achieved by setting $V$ nonzero in (9*b*). As shown in section 2.2, this corresponds qualitatively to the large-disorder Anderson–Hubbard model with $V$ representing an effective nonlocal interaction generated by $U$. Finally, we proceed to explore the effects of the Hartree self-energy due to a nearest-neighbour interaction on the density of states.

### 3.1. Numerical results, $V = 0$

We begin our discussion with the case $V = 0$. In this case, the self-energy is purely local and therefore cannot generate the negative ZBA found in exact numerical calculations. This case is nonetheless interesting because it provides a relatively simple illustration of the role of strong correlations. Throughout this section, strong correlation effects are identified by comparisons between the HFA (which neglects correlations) and HMFT.

The DOS is calculated from the self-consistently determined Green's function via

$$\rho(\omega) = -\frac{1}{N\pi}\sum_i {\rm Im}\, G_{ii}(\omega) \tag{29}$$

where the rank-$N$ matrix $\mathbf{G}(\omega)$ is given by (4). The evolution of $\rho(\omega)$ with doping is shown for $V = 0$ in figure 2. We have chosen $W = 12t$, which corresponds to $W = 1.5D$ where $D = 8t$ is the bandwidth in the clean noninteracting limit. Within HMFT, the AHM is Anderson-localized in two dimensions for this value of $W$ [27]. We have taken $U = 8t$, which is large relative to $t$, but is much less than the critical $U_{\rm c} \approx W$ at which the Mott transition takes place. For comparison, we have shown results for HMFT and for the HI + CPA described in section 2.3. These two theories employ the same approximation for the interaction and differ only in how they treat disorder: nonlocal spatial correlations between impurity sites and the charge density are neglected in effective medium approximations and are treated exactly in HMFT. The two methods give quantitatively similar results, *except* for the ZBA that emerges away from half-filling in HMFT but is absent in HI + CPA.

We note that the sign of the ZBA in figure 2 is positive. This is different from the usual case discussed in the literature, but is consistent with AA theory, where a negative ZBA comes from the exchange self-energy while the Hartree self-energy makes a weak positive correction to the DOS. Since the Hubbard interaction has a vanishing exchange self-energy, the expectation from mean-field theory is for a positive ZBA when $V = 0$. This is illustrated by the numerical HFA calculations shown in figures 2(e)–(h).

Although the sign of the ZBA is the same in HMFT and HFA calculations, its magnitude is different. In particular, the peak at $\varepsilon_{\rm F}$ is finite at all doping levels in the HFA but is absent near half-filling in the HMFT calculations. This difference

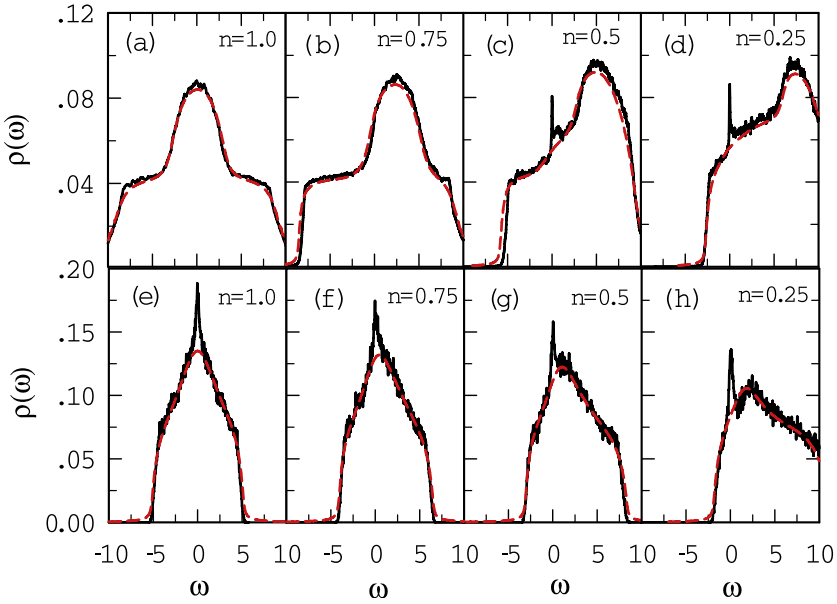


**Figure 2.** Evolution of the DOS with doping for a $12 \times 12$ lattice with $U = 8t$, $W = 12t$, $V = 0$ and 1000–2000 impurity configurations. (a)–(d) Black solid lines and red dashed lines represent the results of HMFT and effective medium calculations, respectively. The Lorentzian broadening is $\gamma = 0.025$ throughout this work. (e)–(h) Corresponding plots for paramagnetic HFA calculations are shown for the same parameters and 1000 impurity configurations.

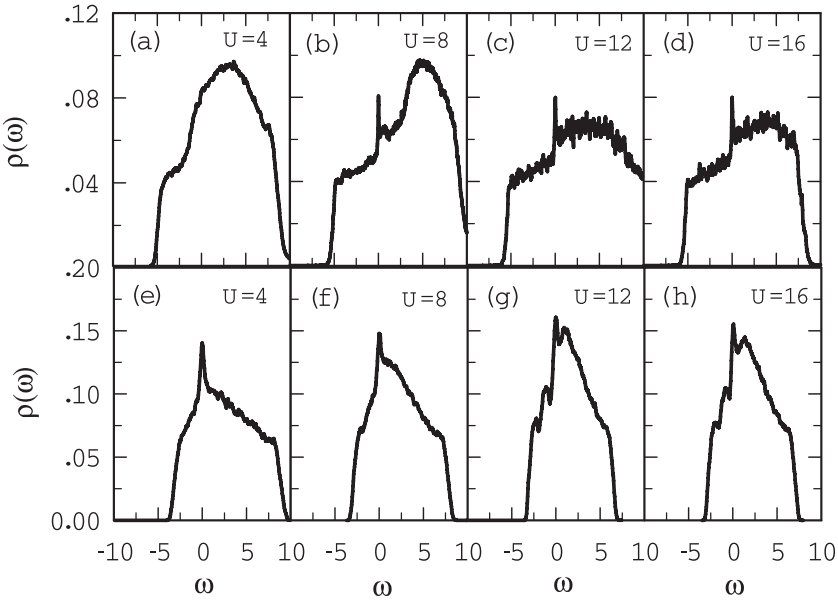


**Figure 3.** Evolution of the DOS with $U$ at quarter-filling for $W = 12t$, $V = 0$, and $8 \times 8$ lattices with 1000 impurity configurations. The upper panels (a)–(d) show HMFT results while the lower panels (e)–(h) show HFA results.

shows that strong correlations suppress the ZBA near half-filling. Results for quarter-filling are shown in figure 3 for a range of $U$, where it can be seen that the ZBA grows with $U$ when $U$ is small, but saturates when $U \gtrsim 8t$. A more technical discussion of these results is given in section 3.3, and we briefly summarize the main ideas of this discussion here.

The main distinction between weakly and strongly correlated systems is that the local charge density $n_i$ is a continuous variable in weakly correlated systems, but is restricted to near-integer values in strongly correlated systems. In the HFA, the energy of an isolated site is $\omega_i = \epsilon_i + Un_i/2$. For sites with $\varepsilon_F - U < \epsilon_i < \varepsilon_F$, the self-consistent equation for the charge density, $n_i = 2f(\omega_i)$ (where $f(x)$ is the Fermi function), will be satisfied at zero temperature by

$$\omega_i = \varepsilon_F, \qquad n_i = 2(\varepsilon_F - \epsilon_i)/U,$$

where the second equality comes from rearranging the expression for $\omega_i$. Since a macroscopic fraction of sites satisfy $\varepsilon_F - U < \epsilon_i < \varepsilon_F$, a peak (i.e. a positive ZBA) is expected in the DOS at the Fermi energy in the atomic limit.

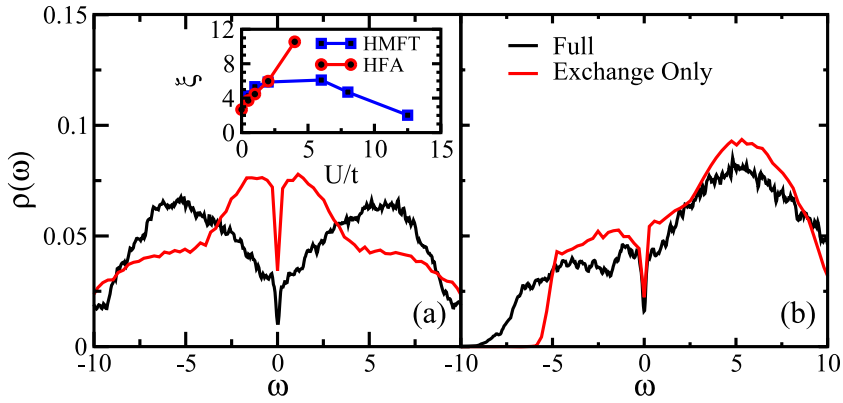


**Figure 4.** Contributions to the zero-bias anomaly for $V = 2.4t$ at (a) half-filling and (b) quarter-filling. For the curve labelled 'full', both the exchange and Hartree self-energy contributions from the nearest-neighbour interaction are retained, while for the curve labelled 'exchange only', the Hartree self-energy is set to zero. The curves show that the ZBA at half-filling comes primarily from the Hartree contribution, and is therefore of the Efros–Shklovskii type. At quarter-filling, the exchange self-energy is dominant and the ZBA is therefore Altshuler–Aronov-like. The inset shows results for the localization length at half-filling reproduced from a finite-size scaling analysis in [27] for $V = 0$. The short localization length at large $U$ in HMFT calculations, relative to HF calculations, is consistent with the enhanced Coulomb gap in the HMFT calculations.

Numerical calculations (not shown) find that the peak persists, but weakens, as $t/W$ grows.

In contrast, the poles in the spectral function for an isolated strongly correlated site are at $\omega_i = \epsilon_i$ and $\omega_i = \epsilon_i + U$. Because of the rigidity of the relationship between $\omega_i$ and $\epsilon_i$, the distribution of $\omega_i$ values follows the distribution of $\epsilon_i$ and a vanishing fraction of sites therefore have resonances at $\varepsilon_F$. There is, consequently, no ZBA when $t = 0$; the ZBA in HMFT calculations only occurs when $t/W$ is nonzero. The discussion in section 3.3 shows that the spectral weight in the ZBA is proportional to the hybridization function $\Lambda_i(\varepsilon_F)$ between sites with $\epsilon_i \approx \varepsilon_F$ or $\epsilon_i + U \approx \varepsilon_F$ and the rest of the lattice. The absence of a ZBA at half-filling comes from the fact that these sites *decouple* from the lattice, i.e. $\Lambda_i(\varepsilon_F) = 0$, when $\varepsilon_F = U/2$.

Our analytical calculations in section 3.3 also suggest that $\Lambda_i(\varepsilon_F)$ is a strong function of both $\varepsilon_F$ and $U$ provided $\varepsilon_F$ lies in the 'central plateau' (by which we mean the broad peak in the DOS arising from the overlap of upper and lower Hubbard bands; see, for example, figure 2(a)). Outside the central plateau, $\Lambda_i(\varepsilon_F)$ is a weak function of both $\varepsilon_F$ and $U$. This is qualitatively consistent with the numerical results in figure 3, which show that the peak height increases with $U$ for $U \lesssim 8t$ and saturates at larger $U$: in the limit $t/W \to 0$, it is easy to show that $\varepsilon_F$ lies in the central plateau for $U < W/2$.

### 3.2. Numerical results, $V \neq 0$

We now consider the case $V \neq 0$. As for $V = 0$, the influence of strong correlations is most visible at half-filling. For the purposes of this discussion, the term 'ES-like behaviour' refers to a negative Hartree contribution to the DOS, and the term 'AA-like behaviour' refers to a Hartree contribution which is positive and an exchange contribution which is negative.

We begin, in figure 4, with a comparison of the effects of the exchange and Hartree self-energies on the ZBA. We argued in section 2.2, based on an examination of the leading-order correction to the local HI self-energy, that an 'exchange-only' treatment of the EAHM could provide a low-energy effective model for the AHM. In such a treatment, only the local self-energy (from $U$) and nonlocal exchange self-energy (from $V$) are present, and $V$ is thought of as an effective interaction originating from $U$, which at half-filling is $V_{\text{eff}} \sim 2t$ (recall (22)). Figure 4 shows that, in the exchange-only calculations, there is a narrow ZBA at $\varepsilon_F$. The ZBA is, by definition, AA-like since it is due to the exchange self-energy. Both the width and depth of the ZBA depend on $V$ (not shown), but both are approximately independent of doping (figures 4(a) and (b)). These results are qualitatively consistent with [28], which found (i) that the shape of the ZBA is roughly doping independent, (ii) that the width scales linearly with $t$, and (iii) that the shape of the ZBA is roughly independent of $W$ and $U$.

The HMFT ZBA is not consistent with unrestricted HFA calculations for the AHM [14–18]. This is not surprising since the physics of the ZBA is different in the two approximations: in HMFT, the ZBA comes from a nonlocal effective interaction generated by spin and charge fluctuations; in the HFA, the ZBA is connected to the formation of static magnetic moments generated by $U$ [17]. One consequence of this difference is that the ZBA is independent of $U$ in HMFT (from (22)) and grows monotonically with $U$ in the HFA.

The residual DOS $\rho(\varepsilon_F)$ is nonzero in our calculations, in contrast to recent results of Shinaoka *et al* [18]. They have shown that, in the unrestricted HFA, there is a soft gap which extends over a narrow energy window $|\omega| \lesssim 0.01t$. A similar soft gap has been found in exact diagonalization calculations in one dimension [18]. However, the widths of these gaps are below the resolution of our calculations, and we are therefore unable to determine whether HMFT predicts a similar soft gap in two dimensions.

We now turn our attention to the Hartree contribution to the self-energy. Figure 4 shows that, at half-filling, it has a

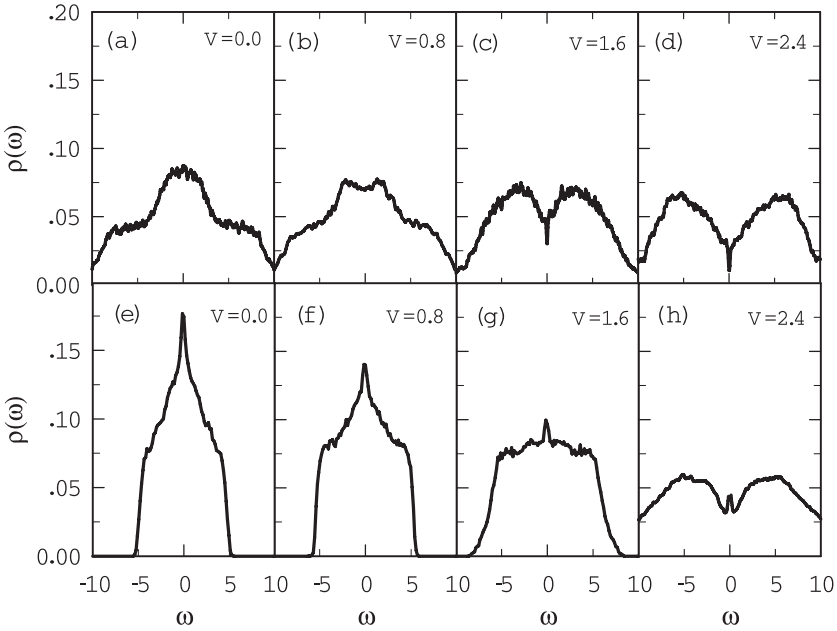


**Figure 5.** Evolution of the DOS with $V$ at half-filling for $U = 8t$ and $W = 12t$. (a)–(d) HMFT results for an $8 \times 8$ lattice with 1000 impurity configurations. (e)–(h) HFA results are for the same parameters and $10 \times 10$ lattices with 1000 impurity configurations.

pronounced effect on the DOS, indicating that the physics of the ZBA in the EAHM is qualitatively different from that in the AHM. The DOS at half-filling is shown in figure 5 for $U = 8t$ and increasing $V$. In both the HMFT and HFA results, ES-like and AA-like behaviour are present. This is most evident in figure 5(d) where the ZBA extends over $-5t \lesssim \omega \lesssim 5t$ and shows a crossover between low- and high-energy behaviour at $|\omega| \approx 0.5t$. That the gap in figure 5(d) is mostly ES-like, except right near the origin, can be seen in figure 4(a) where the full and exchange-only calculations are compared. (Note that the DOS does not satisfy the ES result $\rho(\omega) \propto |\omega - \varepsilon_F|$ because the interaction is short range.)

It was proposed in [42] that there should be a transition between ES-like behaviour farther from the Fermi energy and AA-like behaviour closer in whenever the interaction is finite-ranged. This can be understood following the arguments of ES [1]: in the atomic limit, the average distance between two states near the Fermi energy increases as the difference in their energy decreases. If this distance becomes greater than the range of the interaction, the ES argument breaks down. In our case, the interaction has a finite range, and hence the ES behaviour is lost near the Fermi energy.

The most striking difference between the HMFT and HFA results is the more pronounced ES-like behaviour in the strongly correlated case. Strong correlations result in much less screening of the disorder than in the mean-field treatment, hence enhancing the disorder-driven ES-like behaviour. That the (low-$\omega$) AA-like behaviours in the HMFT and HFA results differ in sign is not surprising given the very different treatment of $U$ in the two cases.

The results at quarter-filling are shown in figure 6. The ZBA in the HMFT results is less pronounced at quarter-filling than at half-filling. The narrow ZBA close to the Fermi energy crosses over from positive to negative, consistent with increasing $V$ and hence increasing negative exchange contribution of the AA type. As seen in figure 6(b), the Hartree self-energy modifies the DOS over a large energy range, but does not produce a gap-like feature at the Fermi energy. Exact studies of small clusters, to be reported elsewhere [32], suggest that the transition from large to small ZBA occurs when $\epsilon_F$ is shifted outside the central plateau described earlier. In the atomic limit, when $\epsilon_F$ lies within the central plateau $n_i$ may have three distinct values (0, 1 or 2), whereas $n_i$ can only be 0 or 1 for $\epsilon_F$ below the lower edge of the plateau. In small clusters, this reduction in the range of possible charge states for individual sites directly results in a reduced ZBA. In marked contrast to the strongly correlated results, the HFA results show an AA-like peak and an ES-like dip, both of which grow with increasing $V$.

Figure 7 shows the variation of the DOS with $U$ for $V = 1.6t$. For the somewhat artificial case of $U = 0$ shown in figures 6(a) and (e), the results differ slightly because the numerical HFA and HMFT routines converge differently. Both obtain charge order frustrated by the disorder, but with slightly shifted domain walls. In the HFA case, increasing $U$ screens the disorder, reducing the ES-like behaviour. The AA-like Hartree peak is initially strengthened by $U$ but is reduced as the screening increases. At large $U$ (figure 7(h)), the DOS approaches the clean-limit result. In the HMFT case, the screening produced by $U$ initially weakens the ES-like behaviour. However, for larger values of $U$, the screening in the strongly correlated case is much less than that in mean field. The localization length based on a finite-size scaling analysis (calculated for $V = 0$) is reproduced from a previous work [27] in the inset of figure 4. While the localization length grows monotonically with $U$ in the HFA, in the HMFT it reaches a maximum at $U \approx 4t$ and decreases with increasing $U$ thereafter. Similarly, the ES-like behaviour of the HMFT

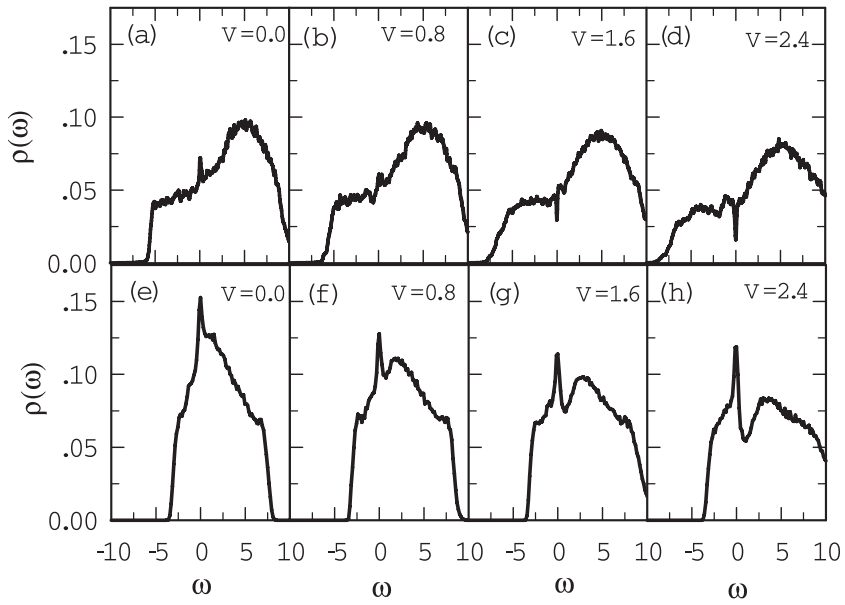


**Figure 6.** Evolution of the DOS with $V$ at quarter-filling with $W = 12t$ and $U = 8t$. Calculations are for an $8 \times 8$ site lattice with more than 1000 sample configurations for each parameter set. Results are shown for (a)–(d) LDFMT and (e)–(h) HFA.

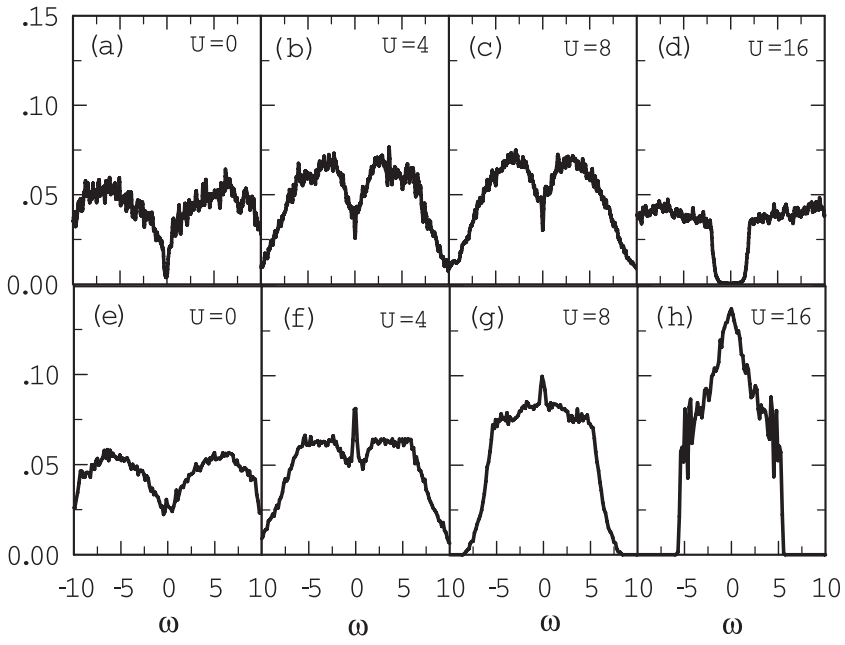


**Figure 7.** Evolution of the DOS with $U$ at half-filling with $W = 12t$ and $V = 1.6t$. (a)–(d) HMFT and (e)–(h) HFA calculations are shown. Calculations are for an $8 \times 8$ site lattice with more than 1000 sample configurations for each parameter set.

DOS is initially weakened, but is not lost as in the HFA and saturates before the opening of the Mott gap.

### *3.3. Analysis of strong correlation effects on the zero-bias anomaly*

In this section, we discuss the origin of the ZBA in the $V = 0$ case. We begin with (4) for the Green's function. In the large-disorder limit, it is possible to treat the hopping matrix element as a perturbation. When the matrix $\mathbf{t}$ is zero, $\mathbf{G}(\omega)$ decouples into a diagonal matrix describing an ensemble of isolated atoms with Green's functions

$$G^0_{ii}(\omega) = \frac{1}{\omega - \epsilon_i - \Sigma^0_{ii}(\omega)}, \tag{30}$$

where the superscript zeros refer to the isolated atomic systems and $\Sigma^0_{ii}(\omega)$ is given exactly by (7). The atomic Green's function, $G^0_{ii}(\omega)$, has poles at

$$\omega^0_{i-} = \epsilon_i; \qquad \omega^0_{i+} = \epsilon_i + U, \tag{31}$$

with spectral weights

$$Z^0_{i-} = 1 - \frac{n_i}{2}; \qquad Z^0_{i+} = \frac{n_i}{2}. \tag{32}$$

The total density of states is found by averaging the imaginary part of $G^0_{ii}(\omega)$ over $\epsilon_i$ in the interval $-W/2 < \epsilon_i < W/2$. Since the pole energies are linear functions of $\epsilon_i$, the total density of states is featureless at the Fermi energy.

Next, we use the fact that the diagonal matrix elements of (4) can be written in the form

$$G_{ii}(\omega) = \frac{1}{\omega - \epsilon_i - \Lambda_i(\omega) - \Sigma_i(\omega)}, \tag{33}$$

where $\Lambda_i(\omega)$ is the hybridization function that describes the coupling of site $i$ to the rest of the lattice. It is

$$\begin{aligned}\Lambda_i(\omega) &= \sum_{jk} t_{ij} t_{ki} G^{(i)}_{jk}(\omega) \\ &\approx t^2 \sum_j G^0_{jj}(\omega)\end{aligned} \tag{34}$$

where $t_{ij}$ are the matrix elements of $\mathbf{t}$ between sites $i$ and $j$, $G^{(i)}_{jk}(\omega)$ is the Green's function for the lattice with site $i$ removed, and the second line is the expansion of the first to $O(t^2)$. Equation (34) applies formally to the limit that the localization length vanishes, but is qualitatively correct for $t \ll W$. We note that $\Lambda_i(\omega)$ is a complex function of frequency for metallic systems, but is real with a discrete spectrum of simple poles for Anderson-localized systems as we have here.

Recalling (7), we solve for the poles of $G_{ii}(\omega)$ to $O(t^2)$:

$$\omega_{i-} = \epsilon_i + \left(1 - \frac{n_i}{2}\right)\Lambda_i(\omega_{i-}), \tag{35a}$$

$$\omega_{i+} = \epsilon_i + U + \frac{n_i}{2}\Lambda_i(\omega_{i+}), \tag{35b}$$

where we have assumed $\Lambda_i \ll U$. In the approximation (34), $\Lambda_i(\omega_{i\pm})$ diverges when $\omega_{i\pm}$ is degenerate with any $\omega_{j\pm}$ for nearest-neighbour site $j$. This is an artefact of the approximation since any degeneracy between $i$ and $j$ is lifted by hybridization of the orbitals. The poles of $\Lambda_i(\omega)$ must therefore differ from $\omega_{i\pm}$ by an energy $\gtrsim t$, and we impose a cutoff $|\Lambda_i(\omega_{i\pm})| < t$.

The spectral weights $Z_{i\pm}$ of the poles (35*a*) and (35*b*) are reduced by $O(t^2)$ from $Z^0_{i\pm}$ and the remaining spectral weight appears at new poles resulting from hybridization of site $i$ with the rest of the lattice. These poles play a role in suppressing the ZBA in the limit that the localization length becomes large, but are of secondary importance when $t \ll W$ as in the current discussion.

Equations (35*a*) and (35*b*) contain the essential physics of the ZBA, which we summarize here before we go into the detailed calculations. In both equations, the local charge susceptibility $\chi_{ii} = -\partial n_i/\partial \epsilon_i$ is nonzero because of the hybridization function $\Lambda_i(\omega)$. The main idea is that, because $\chi_{ii}$ is nonzero, sites with energies $\epsilon_i$ that are sufficiently close to $\varepsilon_F$ ($\varepsilon_F - U$) can adjust their filling $n_i$ such that $\omega_{i-} = \varepsilon_F$ ($\omega_{i+} = \varepsilon_F$). The range of $\epsilon_i$ satisfying the criterion of 'sufficiently close' is set by $\Lambda_i(\varepsilon_F)$, and the weight under the ZBA peak is therefore also set by $\Lambda_i(\varepsilon_F)$. The suppression of the ZBA at half-filling then follows from the fact that the disorder average of $\Lambda_i(\varepsilon_F)$ is an antisymmetric function of $\varepsilon_F$.

We consider sites with energies $\epsilon_i$ such that $\omega_{i\pm} = \varepsilon_F$. The expression for $\omega_{i\pm}$ requires knowledge of the charge density $n_i$, which is given by $n_i/2 = \sum_\pm Z^0_{i\pm} f(\omega_{i\pm}) + O(t^2)$. For sites with $\omega_{i\pm} = \varepsilon_F$, this reduces to [excepting terms of $O(t^2)$]

$$\frac{n_i}{2} = \left(1 - \frac{n_i}{2}\right) f(\varepsilon_F), \qquad (n_i < 1) \tag{36}$$

for $\omega_{i-} = \varepsilon_F$ and

$$\frac{n_i}{2} = \left(1 - \frac{n_i}{2}\right) + \frac{n_i}{2} f(\varepsilon_F), \qquad (n_i > 1) \tag{37}$$

for $\omega_{i+} = \varepsilon_F$. At zero temperature, $0 < f(\varepsilon_F) < 1$ and these equations are satisfied for a range of $\epsilon_i$. Setting $\omega_{i-} = \varepsilon_F$ in (35*a*) and applying the restriction $0 < n_i < 1$, we generate the limits $\epsilon_L < \varepsilon_F - \epsilon_i < \epsilon_U$ on $\epsilon_i$, where

$$\epsilon_L = \min\left(\frac{\Lambda_i(\varepsilon_F)}{2}, \Lambda_i(\varepsilon_F)\right),$$
$$\epsilon_U = \max\left(\frac{\Lambda_i(\varepsilon_F)}{2}, \Lambda_i(\varepsilon_F)\right).$$

In this range (rearranging (35*a*))

$$1 - \frac{n_i}{2} = \frac{\varepsilon_F - \epsilon_i}{\Lambda_i(\varepsilon_F)}, \tag{38}$$

and the density of states at $\varepsilon_F$ coming from sites with $\omega_{i-} = \varepsilon_F$ is therefore

$$\begin{aligned}\delta\rho_-(\omega \approx \varepsilon_F) &= \frac{1}{W}\int_{\varepsilon_F - \epsilon_U}^{\varepsilon_F - \epsilon_L} \mathrm{d}\epsilon_i \, Z_{i-}\delta(\omega - \varepsilon_F) \\ &= \frac{3}{8}\frac{|\Lambda(\varepsilon_F)|}{W}\delta(\omega - \varepsilon_F) + O(t^4).\end{aligned} \tag{39}$$

In this equation, $|\Lambda(\varepsilon_F)|$ is an average over $|\Lambda_i(\varepsilon_F)|$. An identical result can be found for sites with resonance energies $\omega_{i+} = \varepsilon_F$, so that the total density of states near the Fermi energy is

$$\rho(\omega \approx \varepsilon_F) = \frac{3}{4}\frac{|\Lambda(\varepsilon_F)|}{W}\delta(\omega - \varepsilon_F). \tag{40}$$

Equation (40) shows that the ZBA is a delta function at zero temperature. At finite temperatures $T$, the ZBA is a peak of width $\sim T$. The spectral weight in the peak is proportional to the hybridization function $\Lambda(\varepsilon_F)$, and we next show how this depends on doping.

We consider a site $i$ in a lattice with coordination number $Z_c$, whose nearest neighbours have randomly chosen site energies. At half-filling ($\varepsilon_F = U/2$), the terms $G^0_{jj}(\varepsilon_F)$ in the sum in (34) are positive or negative with equal probability, and tend to cancel. As the filling is reduced, the probability that $G^0_{jj}(\varepsilon_F)$ is negative (positive) becomes larger (smaller). We make a rough calculation that illustrates this behaviour by replacing the sum over site index $j$ in (34) with an integral over $\epsilon_j$. Thus

$$\Lambda_i(\varepsilon_F) \approx \frac{t^2 Z_c}{W}\int_{-W/2}^{W/2} \mathrm{d}\epsilon \left(\frac{1 - n_\epsilon/2}{\varepsilon_F - \epsilon} + \frac{n_\epsilon/2}{\varepsilon_F - \epsilon - U}\right),$$

where $n_\epsilon$ is the charge density for sites with site energy $\epsilon$. Recalling our constraint $|\Lambda_i(\varepsilon_F)| \lesssim t$, we introduce cutoffs near the poles of the integrand. Noting that

$$n_\epsilon = \begin{cases} 2, & \epsilon < \varepsilon_F - U \\ 1, & \varepsilon_F - U < \epsilon < \varepsilon_F \\ 0, & \epsilon > \varepsilon_F \end{cases}$$

we get

$$\Lambda_i(\varepsilon_F) \approx \frac{t^2 Z_c}{W} \ln\left(\frac{\frac{W}{2} + \varepsilon_F - U}{\frac{W}{2} - \varepsilon_F}\right), \tag{41a}$$

for $U - \frac{W}{2} < \varepsilon_F < \frac{W}{2}$ and

$$\Lambda_i(\varepsilon_F) \approx \frac{t^2 Z_c}{W}\left[\ln\left(\frac{\frac{W}{2} + \varepsilon_F}{\frac{W}{2} - \varepsilon_F}\right) + \frac{1}{2}\ln\left(\frac{U - \frac{W}{2} - \varepsilon_F}{\frac{W}{2} + \varepsilon_F}\right) + \frac{1}{2}\ln\left(\frac{t}{U}\right)\right] \tag{41b}$$

for $-\frac{W}{2} < \varepsilon_F < U - \frac{W}{2}$. The logarithmic divergences in (41*a*) and (41*b*) are artificial and must be cut off whenever any numerator or denominator has a magnitude smaller than $t$. Equation (41*a*) applies when the Fermi level sits in the central plateau, and shows that $\Lambda_i(\varepsilon_F)$ is antisymmetric about half-filling (i.e. $\varepsilon_F = U/2$), and grows linearly away from half-filling. Outside of the central plateau, $\Lambda_i(\varepsilon_F)$ is a weak function of $\varepsilon_F$.

In order to compare with figure 3, we evaluate (41*b*) at quarter-filling, which for small $t$ corresponds to

$$\varepsilon_F \approx \begin{cases} \frac{U}{2} - \frac{W}{4}, & U < \frac{W}{2} \\ 0, & U > \frac{W}{2}. \end{cases}$$

Then (41*b*) gives

$$|\Lambda_i(\varepsilon_F)| \approx \frac{t^2 Z_c}{W}\left[\ln\left(\frac{\sqrt{(\frac{W}{2})^2 - U^2}}{\frac{3}{2}W - U}\right) - \frac{1}{2}\ln\left(\frac{U}{t}\right)\right], \tag{42a}$$

for $U < \frac{W}{2}$, and

$$|\Lambda_i(\varepsilon_F)| \approx \frac{t^2 Z_c}{2W}\left[\ln\left(\frac{2U - W}{W}\right) - \ln\left(\frac{U}{t}\right)\right], \tag{42b}$$

for $U > \frac{W}{2}$. In (42*a*), $|\Lambda_i(\varepsilon_F)|$ grows linearly with $U$ for small $U$ (recall that there is a cutoff such that $\ln(U/t) \to \ln(t/t)$ when $U < t$), and saturates at a finite value when $U \gg \frac{W}{2}$. Both these results, and the results at half-filling in (41*a*) are qualitatively consistent with the numerical results shown in figures 2 and 3.

## 4. Conclusions

We have studied the effects of strong correlations on the disorder-induced zero-bias anomaly in the density of states for disordered interacting systems in two dimensions. A purely local self-energy fails to capture the true physics, demonstrating the importance of nonlocal contributions to the self-energy in this context. We have motivated analytically and demonstrated numerically that including an exchange self-energy generates a doping independent ZBA as seen in other studies of the Anderson–Hubbard model. In the extended Anderson–Hubbard model, strong correlations suppress screening strengthening Efros–Shklovskii-like behaviour and greatly enhancing the ZBA. Because strong correlations are less important at quarter-filling than at half-filling, the zero-bias anomaly in the extended Anderson–Hubbard model shows strong doping dependence.

## Acknowledgments

We acknowledge financial support from NSERC of Canada, Canada Foundation for Innovation, Ontario Innovation Trust, and the DFG (SFB 484). Some calculations were performed on the High Performance Computing Virtual Laboratory (HPCVL).

## References

[1] Efros A L and Shklovskii B I 1975 *J. Phys. C: Solid State Phys.* **8** L49
[2] Efros A L 1976 *J. Phys. C: Solid State Phys.* **9** 2021
[3] Altshuler B L and Aronov A G 1985 *Modern Problems in Condensed Matter Sciences* vol 10 (Amsterdam: North-Holland)
[4] Butko V Yu, DiTusa J F and Adams P W 2000 *Phys. Rev. Lett.* **84** 1543–6
[5] Dagotto E 1994 *Rev. Mod. Phys.* **66** 763–840
[6] Imada M, Fujimori A and Tokura Y 1998 *Rev. Mod. Phys.* **70** 1039–263
[7] Morin F J 1959 *Phys. Rev. Lett.* **3** 34–6
[8] Hanasaki N, Kinuhara M, Kézsmárki I, Iguchi S, Miyasaka S, Takeshita N, Terakura C, Takagi H and Tokura Y 2006 *Phys. Rev. Lett.* **96** 116403
[9] Sarma D D, Chainani A, Krishnakumar S R, Vescovo E, Carbone C, Eberhardt W, Rader O, Jung Ch, Hellwig Ch, Gudat W, Srikanth H and Raychaudhuri A K 1998 *Phys. Rev. Lett.* **80** 4004–7
[10] Ino A, Okane T, Fujimori S-I, Fujimori A, Mizokawa T, Yasui Y, Nishikawa T and Sato M 2004 *Phys. Rev.* B **69** 195116
[11] Kim J, Kim J Y, Park B G and Oh S J 2006 *Phys. Rev.* B **73** 235109
[12] Nakatsuji S, Dobrosavljevic V, Tanaskovic D, Minakata M, Fukazawa H and Maeno Y 2004 *Phys. Rev. Lett.* **93** 146401
[13] Kim K W, Lee J S, Noh T W, Lee S R and Char K 2005 *Phys. Rev.* B **71** 125104
[14] Milovanović M, Sachdev S and Bhatt R N 1989 *Phys. Rev. Lett.* **63** 82–5
[15] Tusch M A and Logan D E 1993 *Phys. Rev.* B **48** 14843–58
[16] Heidarian D and Trivedi N 2004 *Phys. Rev. Lett.* **93** 126401
[17] Fazileh F, Gooding R J, Atkinson W A and Johnston D C 2006 *Phys. Rev. Lett.* **96** 046410
[18] Shinaoka H and Imada M 2009 *Phys. Rev. Lett.* **102** 016404
[19] Ulmke M, Janiš V and Vollhardt D 1995 *Phys. Rev.* B **51** 10411–26
[20] Laad M S, Craco L and Müller-Hartmann E 2001 *Phys. Rev.* B **64** 195114
[21] Dobrosavljević V, Pastor A A and Nikolić B K 2003 *Europhys. Lett.* **62** 76
[22] Byczuk K, Hofstetter W and Vollhardt D 2005 *Phys. Rev. Lett.* **94** 056404
[23] Balzer M and Potthoff M 2005 *Physica* B **359–361** 768–70

[24] Lombardo P, Hayn R and Japaridze G I 2006 *Phys. Rev.* B **74** 085116
[25] Dobrosavljević V and Kotliar G 1997 *Phys. Rev. Lett.* **78** 3943
[26] Miranda E and Dobrosavljević V 2005 *Rep. Prog. Phys.* **68** 2337
[27] Song Y, Atkinson W A and Wortis R 2008 *Phys. Rev.* B **77** 054202
[28] Chiesa S, Chakraborty P B, Pickett W E and Scalettar R T 2008 *Phys. Rev. Lett.* **101** 086401
[29] Freericks J K 2004 *Phys. Rev.* B **70** 195342
Okamoto S and Millis A J 2004 *Phys. Rev.* B **70** 241104(R)
Lee W-C and MacDonald A H 2006 *Phys. Rev.* B **74** 075106
Yunoki S, Moreo A, Dagotto E, Okamoto S, Kancharla S S and Fujimori A 2007 *Phys. Rev.* B **76** 064532
[30] Georges A, Kotliar G, Krauth W and Rozenberg M J 1996 *Rev. Mod. Phys.* **68** 13
[31] Zhang Y Z and Imada M 2007 *Phys. Rev.* B **76** 045108
[32] Chen H, Wortis R and Atkinson W A, unpublished
[33] Fulde P 1995 *Springer Series in Solid State Sciences* vol 100 (Berlin: Springer)
[34] Mehlig B, Eskes H, Hayn R and Meinders M B J 1995 *Phys. Rev.* B **52** 2463–70
[35] Gröber C, Eder R and Hanke W 2000 *Phys. Rev.* B **62** 4336–52
[36] Mancini F and Avella A 2004 *Adv. Phys.* 537
[37] Abrahams E, Anderson P W, Lee P A and Ramakrishnan T V 1981 *Phys. Rev.* B **24** 6783–9
[38] Lieb E H and Wu F Y 1968 *Phys. Rev. Lett.* **20** 1445–8
[39] Hirsch J E 1985 *Phys. Rev.* B **31** 4403–19
[40] White S R, Scalapino D J, Sugar R L, Loh E Y, Gubernatis J E and Scalettar R T 1989 *Phys. Rev.* B **40** 506–16
[41] Otsuka Y and Hatsugai Y 2000 *J. Phys.: Condens. Matter* **12** 9317–22
[42] Epperlein F, Schreiber M and Vojta T 1997 *Phys. Rev.* B **56** 5890–6